

Metal-Based Bio-Active Pyrazole Derivatives: Preparation, Spectral, Thermal, Photophysical, and Antimicrobial Studies

Dr. Priyanka Devi ^{1,*}, Kiran Singh ^{2,*}

¹ Department of Chemistry, Kurukshetra University, Kurukshetra – 136119, India

² Department of Chemistry, JCD Vidyapeeth, Sirsa – 125110, India

* Correspondence: niraniap@gmail.com (P.D.); knsingh@kuk.ac.in (K.S.);

Received: 30.11.2023; Accepted: 7.05.2025; Published: 25.11.2025

Abstract: A new bioactive Schiff base named 3-methyl-1-phenyl-5-((5-bromosalicylidene) amino)-pyrazole was prepared by condensing 5-amino-3-methyl-1-phenylpyrazole with 5-bromosalicylaldehyde in methanol on a heating mantle in refluxing conditions for 1 hour. The synthesized Schiff base was characterized by ¹H-NMR and IR spectroscopy. The Co²⁺, Ni²⁺, Cu²⁺, and Zn²⁺ metal complexes of the Schiff base in (1:1) and (1:2) have also been prepared by condensing the metal acetate salt with the synthesized Schiff base. The prepared metal complexes were characterized by various physicochemical techniques, including ¹H-NMR, IR, mass spectrometry, elemental analysis, UV-Vis, Cyclic voltammetry, electronic spectra, and Electron spin resonance. The presence of coordinated water molecules in the complexes has been calculated with the help of thermogravimetric analysis. Fluorescence spectra of all the compounds showed an enhancement in the fluorescence intensity of the metal complexes compared to the Schiff base. Square-planar geometry for the copper complexes and octahedral geometry for the cobalt, nickel, and zinc metal complexes have been proposed using different techniques. The biological activity of all the compounds was assessed, and the results showed that the metal complexes exhibited greater biological activity than the ligand.

Keywords: fluorescence; characterization; thermogravimetric analysis; physicochemical techniques; metal complex; coordinated water.

© 2025 by the authors. This article is an open-access article distributed under the terms and conditions of the Creative Commons Attribution (CC BY) license (<https://creativecommons.org/licenses/by/4.0/>), which permits unrestricted use, distribution, and reproduction in any medium, provided the original work is properly cited. The authors retain copyright of their work, and no permission is required from the authors or the publisher to reuse or distribute this article, as long as proper attribution is given to the original source.

1. Introduction

Antibiotics, antimicrobial drugs, and anti-infectious agents are used to treat infectious diseases caused by microorganisms and can kill or inhibit the growth of microbes by inhibiting cell membrane synthesis, protein synthesis, nucleic acid synthesis, or cytoplasmic membranes [1,2]. Lately, the opposition of microorganisms to antibiotics has been recognized and classified into intrinsic resistance and acquired resistance [3]. The inactivation of medications by bacterial catalysts, or the inability of the medication to bind to the reasons that make sense of the biochemical mechanisms of internal and acquired resistances [4,5]. Thus, there is an urgent need to develop new antimicrobial medications or repurpose existing ones to counter the evolution of microorganisms and address resistance. Schiff bases (bearing an imine or azomethine (-HC=N-) group) have shown a wide range of activities, including anti-diabetic

activity, catalytic activity, DNA binding, cleavage activity, and cytotoxicity [6]. Furthermore, several reports highlight the significance of Schiff bases as antimicrobial agents [7–9].

Pyrazoles are generally used as core motifs in numerous compounds for applications such as catalysis, agro-synthetic products, building blocks for various mixtures, and medicine [10,11]. The versatility of pyrazoles and their derivatives, which enables the synthesis of a variety of analogs with diverse moieties, makes them appealing, as they can alter the electronic properties and, consequently, the characteristics of the resulting compounds [12]. In medicine, pyrazoles are found as pharmacophores in a portion of active biological molecules [13]. While pyrazole derivatives have been widely studied for various applications, including anticancer, antimicrobial, anti-glycemic, anti-inflammatory, anti-allergy, and antiviral, significantly less has been reported about their metal counterparts, notwithstanding the way metals have been shown to impart activity to ligands [10]. Consequently, this viewpoint is expected to highlight the capabilities of pyrazole and pyrazolyl metal complexes in the field of drug discovery and development [14]. A few models that incorporate palladium, platinum, copper, gold, zinc, cobalt, nickel, iron, silver, and gallium complexes are used to support the above point [10].

Schiff bases are characterized by the presence of an imine bond in their structure and are built up from aldehydes with essential amines [15]. These compounds have a wide range of applications, including pharmaceutical, industrial, fungicidal, bactericidal, antiviral, and biological applications [16–18]. Over recent years, there has been impressive interest among researchers in the synthesis and characterization of metal complexes, like Co(II), Ni(II), Cu(II), and Zn(II), made out of Schiff bases (utilized as ligands) because of their large number of uses in the pharmaceutical field [19–21]. Complexes containing oxygen or potentially nitrogen, for example, Lewis bases, certainly receive sufficient attention in the field by virtue of their great structural diversity, sensitivity to the molecular environment, and thermodynamic stability [22,23]. The synthesis and structural analyses of polydentate Schiff bases and their metal complexes have shown that these materials exhibit a wide range of structural and physicochemical properties [24,25]. Comprehensive studies of these compounds are necessary to understand their structure-property correlations better and to maximize and rationalize their use. This is due to the structural simplicity of polydentate Schiff bases and their metal complexes, and to the ease with which they can be obtained [26,27].

In metal-based pharmaceuticals, the metal may coordinate ligands via oxygen, nitrogen, and sulfur donor atoms, forming a precise three-dimensional structure that allows the molecule to be tailored to identify and interact with a specific molecular target [28]. This is further boosted by various chemical modifications, such as inserting different groups onto ligands. However, the tremendous flexibility of coordination geometry, which is exclusively dictated by steric hindrance and ligand charge, allows for a transition between alternative configurations [29]. First-row transition metal complexes have been recognized for their biological actions, including antibacterial, antifungal, anticonvulsant, anti-diabetic, anti-inflammatory, antioxidant, and antiproliferative/antitumor activities [30–32].

2. Materials and Methods

After purchase from Sigma-Aldrich, all chemicals were used without further purification. The formation of the product was checked with TLC. The infrared spectral data for all the compounds were obtained using a Perkin-Elmer Spectrum 2 spectrometer. Data for elemental analysis were collected at IIT Bombay using a Perkin-Elmer (2400) elemental analyzer. The $^1\text{H-NMR}$ spectra for the confirmation of the formation of Schiff base and its zinc

metal complexes were evaluated in DMSO-d₆ on a 400 MHz JOEL spectrometer at Kurukshetra University, Kurukshetra. The absorption spectra of the metal complexes have been studied in the 200-700 nm region on a LABINDIA UV/VIS spectrophotometer. The emission spectra of the compounds were recorded on a SHIMADZU spectrofluorometer in DMSO. A three-electrode system, i.e., Iviam Stat (IV) Electro synthetic analyzer, was used to study the electrochemical behavior of the copper complexes using KCl as the supporting electrolyte. Electron spin resonance spectra of the copper complexes were obtained to determine the geometry and electronic arrangement around the metal ion using a Varian (E-112) ESR spectrometer. The thermal gravimetric analysis of the 1:1 metal complex was performed on a TG/DTA 7300 of EXSTAR with a heating rate of 10°C/min in the temperature range of 40-1000°C. All the compounds were evaluated for biological activity using the agar well diffusion method. Metal contents in the prepared complexes were determined by gravimetric analysis: Zn as zinc ammonium phosphate, cobalt as cobalt pyridine thiocyanate, copper as cuprous thiocyanate, and nickel as nickel (dmg) dimethylglyoximate.

3. Results and Discussion

3.1. Synthesis of Schiff base.

The novel Schiff base was prepared by refluxing a 1:1 molar ratio of 5-amino-3-methyl-1-phenylpyrazole with 5-bromosalicylaldehyde in 15 mL of methanol in a 25 mL round-bottom flask for 2 hours. The progress of the reaction mixture was checked by thin-layer chromatography (TLC) using hexane:ethyl acetate (70:30). The yellow precipitate was filtered and recrystallized from methanol. The recrystallized solid was washed with acetone and dried in a vacuum desiccator. The melting point of the Schiff base was found to be 194°C. The synthesized Schiff base was characterized by ¹H-NMR and IR spectroscopy (Figure 1).

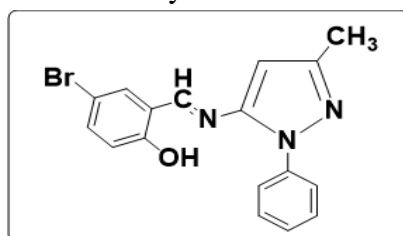


Figure 1. Structure of Schiff base

3.1.1. Synthesis of metal complexes.

The 1:1 and 1:2 metal complexes of the new Schiff base have been prepared. The 1:1 metal complex was prepared by adding a 1:1 molar ratio of Schiff base to the metal acetate salt in methanol under refluxing conditions on a heating mantle for 3 hours. For 1:2 metal complexes, a Schiff base and a metal acetate salt in a 2:1 molar ratio were refluxed with the metal for 4 hours. TLC studied the formation of the metal complexes. The solid precipitates were filtered, washed with acetone, and finally dried in a vacuum desiccator over calcium chloride. The melting point of all the metal complexes was noted down. Different physicochemical techniques characterized all the metal complexes.

3.2. Elemental analysis.

The formation of the colored metal complexes in 1:1 and 1:2 molar ratios was confirmed by elemental data (Figure 2). The metal complexes are mainly soluble in DMSO,

DMF, and THF but are insoluble in methanol and ethanol. The newly synthesized compounds are solid, non-hygroscopic, and decompose at high temperatures (Table 1).

Table 1. Elemental data of the compounds.

Compounds	Mol. weight	Melting point (°C)	Color	Yield (%)	Elemental Analysis (%) Cald.			Metal (%) Cald. (Found)
					C	H	N	
Schiff Base	356.22	194	Pale Yellow	81	57.32 (57.16)	3.96 (3.80)	11.80 (11.66)	
Co(1:1)	527.23	234	Brown	85	43.28 (43.23)	4.21 (4.37)	7.97 (7.82)	11.18 (11.27)
Co(1:2)	805.39	240	Brown	78	50.70 (50.54)	3.75 (3.99)	10.43 (14.67)	7.32 (7.19)
Ni(1:1)	526.99	242	Reddish	80	43.30 (43.19)	4.21 (4.37)	7.97 (7.89)	11.14 (11.03)
Ni(1:2)	805.15	245	Reddish	76	50.72 (50.63)	3.76 (3.83)	10.44 (10.35)	7.29 (7.19)
Cu(1:1)	495.82	220	Green	79	46.03 (46.14)	3.66 (3.79)	8.48 (8.58)	12.82 (12.75)
Cu(1:2)	773.97	223	Green	81	52.76 (52.79)	3.39 (3.52)	10.86 (10.72)	8.21 (8.07)
Zn(1:1)	533.68	250	Light Yellow	86	42.76 (42.85)	4.16 (4.29)	7.87 (7.96)	12.25 (12.17)
Zn(1:2)	811.84	252	Light Yellow	87	50.30 (50.52)	3.72 (3.63)	10.35 (10.21)	8.05 (8.18)

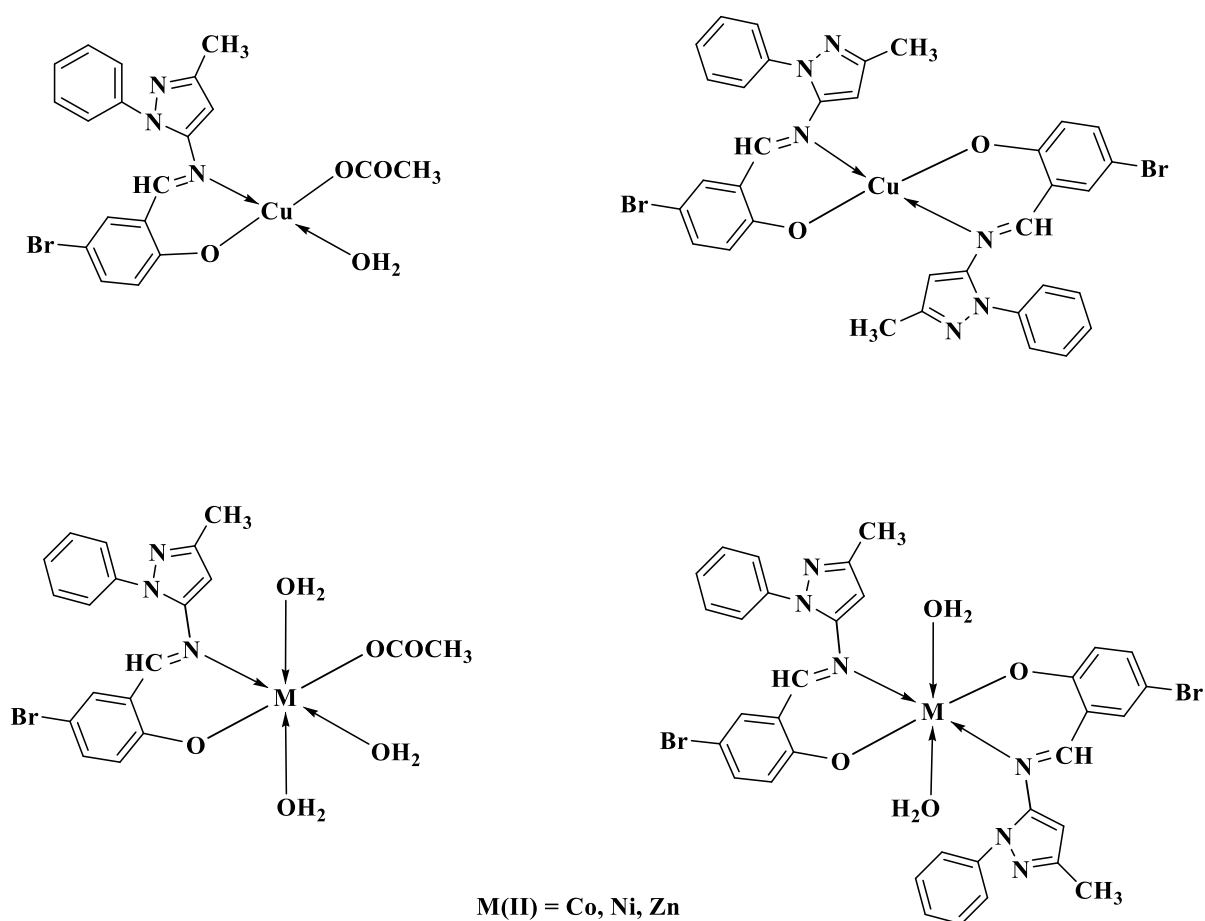


Figure 2. Proposed structures of the metal complexes.

3.3. IR spectra.

All the metal complexes were first characterized by infrared spectroscopy in the range of 400-4000 cm^{-1} . A band appears at 1609 cm^{-1} due to the azomethine moiety of the Schiff base, and the value of this band gets lowered in the spectra of metal complexes due to the coordination of the metal ion with the nitrogen atom of the imine group [33]. Another band at 3345 cm^{-1} appeared due to the hydroxy group of the salicylaldehyde moiety in the Schiff base [34]. This band shifted in the lower region of 13-40 cm^{-1} , which confirms the bonding of metal ions with the oxygen of the hydroxy group [35]. New bands in the range of 3408-3494 cm^{-1} appeared due to the coordinated water molecules in the metal complexes [36]. New bands in the range of 1729-1740 cm^{-1} appeared due to the acetate group in a 1:1 metal complex (Table 2). Another band in the region 1315-1382 cm^{-1} exhibited due to the (C-O) bond [37]. Two new bands in the regions 442-481 and 510-582 cm^{-1} appeared due to metal-nitrogen and metal-oxygen bonds, respectively, confirming the formation of metal complexes [38].

Table 2. IR spectral data of the ligand and complexes.

Compounds	$\nu(-\text{HC}=\text{N}-)$	$\nu(\text{OH})$	$\nu(\text{OCOCH}_3)$	$\nu(\text{H}_2\text{O})$	$\nu(\text{M}-\text{O})$	$\nu(\text{M}-\text{N})$
Ligand	1609	3345	-	-	-	-
Co(1:1)	1569	-	1729	3408	465	548
Co(1:2)	1570	-	-	3456	475	548
Ni(1:1)	1585	-	1730	3494	481	582
Ni(1:2)	1596	-	-	3578	447	567
Cu(1:1)	1590	-	1740	3472	451	519
Cu(1:2)	1571	-	-	-	447	524
Zn(1:1)	1590	-	1738	3488	442	519
Zn(1:2)	1591	-	-	3467	461	510

3.4. $^1\text{H-NMR}$ spectra.

The $^1\text{H-NMR}$ spectra of the **HL-5** and its zinc metal complexes were recorded to confirm the formation of the ligand and its zinc metal complexes. The Schiff base showed a singlet at 2.22 ppm due to the protons of the pyrazole -CH₃ group (Figure 3). The characteristic signal for the -HC=N proton appeared at 9.15 ppm, which shifted in the spectra of zinc metal complexes, indicating coordination of the nitrogen of the imine group to the metal ions [39]. A broad signal at 12.50 ppm was observed due to the -OH proton, which disappeared in the spectra of metal complexes due to the complexation of the oxygen (Figure 4) of the hydroxy group with the zinc metal ions [40]. The signals for aromatic protons appeared in the range of 7.04-8.58 ppm in the spectra of the compounds [41]. A singlet at 6.50 ppm appeared due to the -CH proton of the pyrazole ring (Figure 5). The proton signals for another aromatic ring appeared in the range of 7.33-7.60 ppm in the spectra of the compounds (Table 3).

Table 3. $^1\text{H-NMR}$ spectral data of the compounds.

Compounds	δ (ppm)
HL	12.50 (s, 1H, -OH), 9.15 (s, 1H, -HC=N), 7.08 (d, 1H, Ar-H), 8.20 (d, 1H, Ar-H), 8.58 (s, 1H, Ar-H), 7.37-7.60 (m, 5H, Ar-H), 6.50 (s, 1H, -CH of Py), 2.22 (s, 3H, CH ₃)
Zn (1:1)	9.08 (s, 1H, -HC=N), 7.06 (d, 1H, Ar-H), 8.20 (d, 1H, Ar-H), 8.58 (s, 1H, Ar-H), 7.35-7.58 (m, 5H, Ar-H), 6.50 (s, 1H, -CH of Py), 2.24 (s, 3H, CH ₃), 3.29 (s, 3H, CH ₃ COO)
Zn (1:2)	9.09 (s, 1H, -HC=N), 7.04 (d, 1H, Ar-H), 8.19 (d, 1H, Ar-H), 8.57 (s, 1H, Ar-H), 7.33-7.58 (m, 5H, Ar-H), 6.49 (s, 1H, -CH of Py), 2.24 (s, 3H, CH ₃)

HL-5

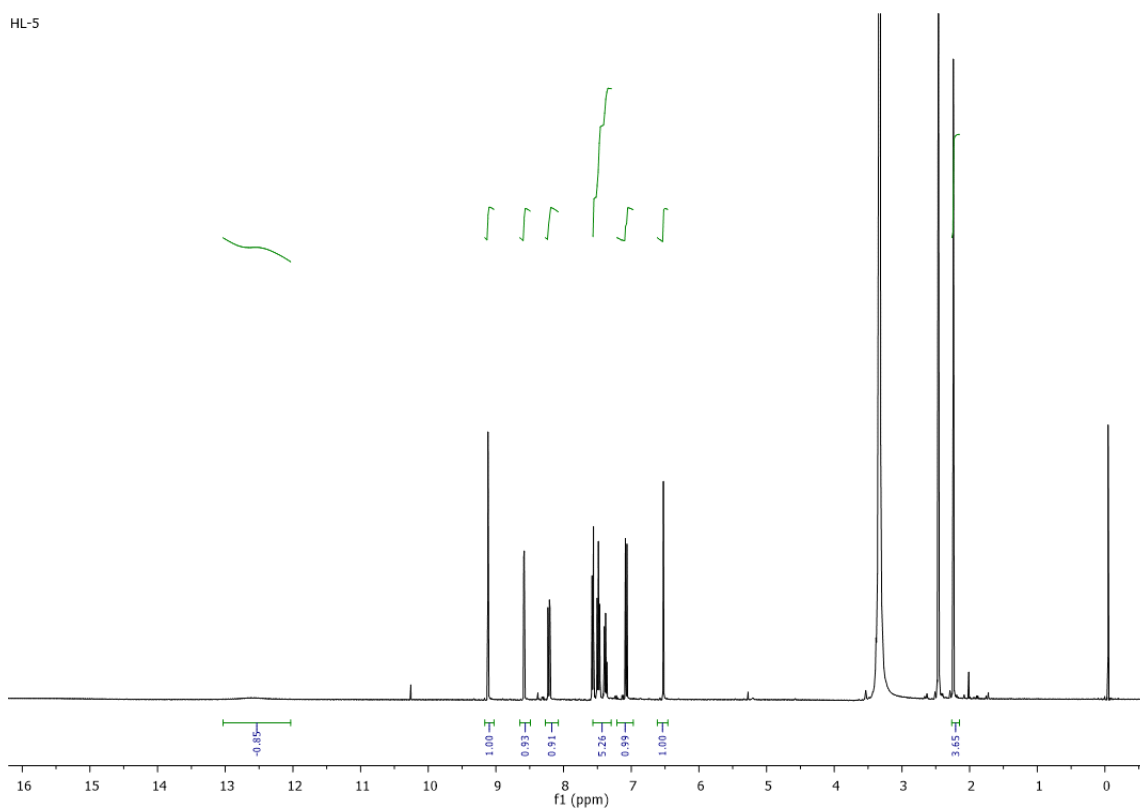


Figure 3. Proton-NMR spectrum of the ligand.

Zn:L-5(1:1)

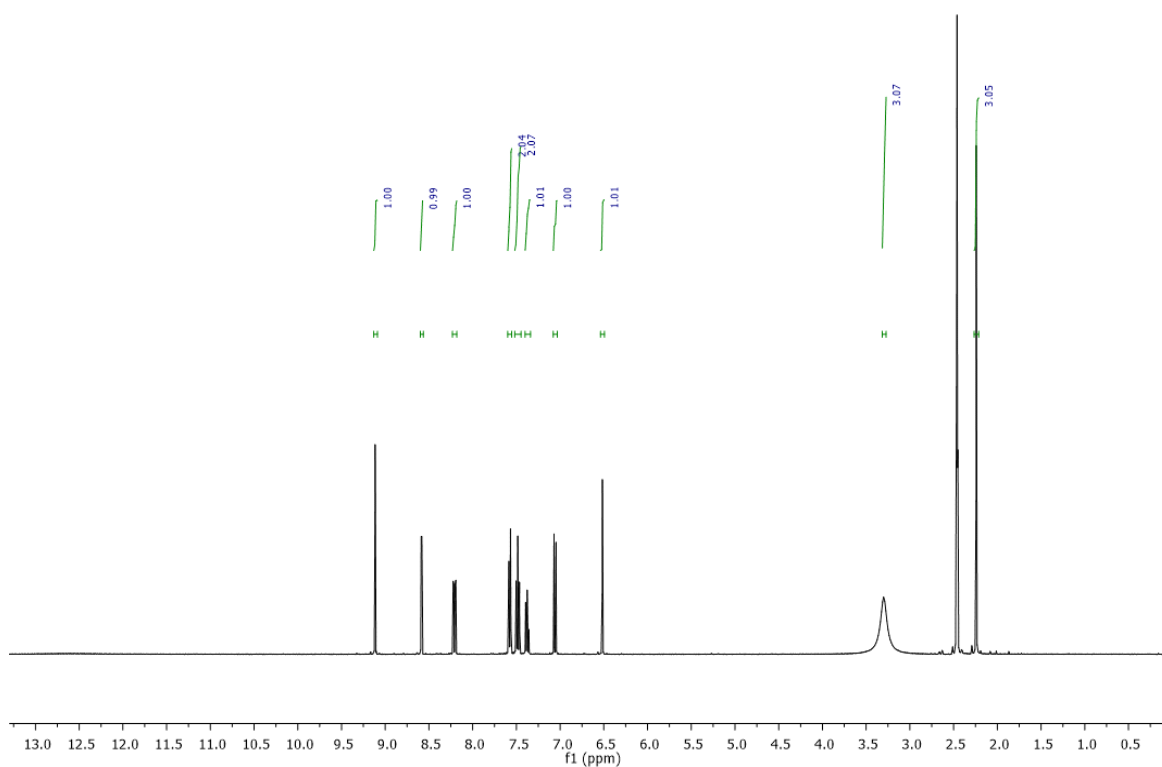


Figure 4. Proton-NMR spectrum of the (1:1) zinc complex.

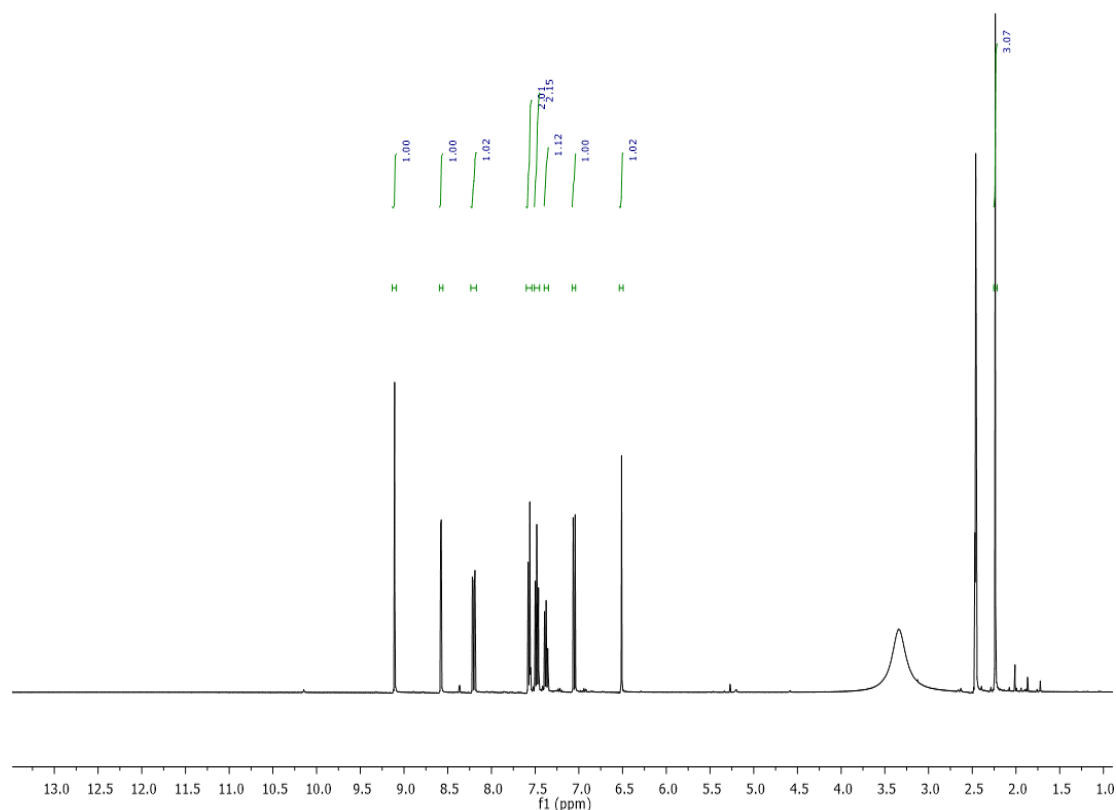


Figure 5. Proton-NMR spectrum of the (1:2) zinc complex.

3.5. Electronic spectra.

Electronic spectra have been recorded in DMSO at a concentration of 10⁻⁵ M to determine the number and positions of the d-d transitions, the electronic environment, and the stereochemistry of the Schiff base around the metal ions.

3.5.1. Cobalt 1:1 and 1:2 metal complexes.

Two transitions were detected in the electronic spectra of metal complexes, i.e., 12570-12670 (ν_1) and 21504-22311 (ν_3) cm^{-1} , analogous to the ${}^4\text{T}_{1g}(\text{F}) \rightarrow {}^4\text{T}_{2g}(\text{F})$ and ${}^4\text{T}_{1g}(\text{F}) \rightarrow {}^4\text{T}_{1g}(\text{P})$ transitions, respectively. The observed magnetic moment values were in the range of 4.56-4.86 B.M. The observed magnetic moments and band positions indicate an octahedral geometry for both cobalt metal complexes. The ν_2 was not observed; it was calculated using the equation $\nu_2 = \nu_1 + 10Dq$. The ratio of the second to first transition (ν_2/ν_1) is 2.09 (1:1) and 2.10 (1:2), indicating an octahedral geometry around the cobalt complexes [42]. The value of crystal field quantities (Dq , B , ν_2/ν_1 , β , and $\beta\%$) was also calculated. The values of β for both the complexes are 677.1 (1:1) and 728.9 cm^{-1} (1:2), which are less than 971 cm^{-1} , indicating the metal-ligand orbital overlapping and delocalization of the electrons on the cobalt metal center. The deviation of values of nephelauxetic parameters from unity indicates the covalent character of the metal-ligand bonds (Table 4).

Table 4. Electronic data of the metal complexes.

Complexes	Transitions (cm^{-1})			Dq (cm^{-1})	B (cm^{-1})	ν_2/ν_1	β	β (%)
	ν_1	ν_2	ν_3					
Co(1:1)	12570	26374*	21504	1380	677.1	2.09	0.698	30.2
Co(1:2)	12670	26633*	22311	1396	728.9	2.10	0.750	24.9

Complexes	Transitions (cm ⁻¹)			Dq (cm ⁻¹)	B (cm ⁻¹)	ν ₂ /ν ₁	β	β (%)
	ν ₁	ν ₂	ν ₃					
Ni(1:1)	10197	17693	23612	1019	714.3	1.73	0.686	31.4
Ni(1:2)	10298	17979	23999	1029	738.9	1.74	0.709	29.1
Cu(1:1)	17519							
Cu(1:2)	19547							

3.5.2. Nickel 1:1 and 1:2 metal complexes.

For nickel complexes, three absorption bands are observed in the range of 10197-10298 (ν₁), 17693-17979(ν₂) and 23612-23999 (ν₃) cm⁻¹ assigned for the spin allowed ³A_{2g}(F) → ³T_{2g}(F), ³A_{2g}(F) → ³T_{1g}(F) and ³A_{2g}(F) → ³T_{1g}(P) transitions, respectively. The ligand field parameters were calculated for both nickel complexes. The observed magnetic moment values for the nickel complexes are in the range of 3.443-4.8 B.M. The values of ligand-field parameters, magnetic moments, and the range of transitions indicate an octahedral geometry around the nickel metal center [43]. All the parameters Dq, B, ν₂/ν₁, β, and β% are displayed in the table below. The ratio ν₂/ν₁ in the range of 1.73-1.74 favors the octahedral geometry around the nickel metal center [44]. The values of the Racah parameter were less than 1041 cm⁻¹, indicating the covalent nature of the metal-ligand bond. The values of β in (0.686 for 1:1 complex and 0.709 for 1:2 complex) close to 0.50 indicate a more covalent character in the nickel complexes than cobalt complexes [45,46]. The β% values are in good agreement with the overlap of metal-ligand orbitals.

3.5.3. Copper 1:1 and 1:2 metal complexes.

The copper complexes showed a solitary broad band in the range of 17519-19547 cm⁻¹, which was assigned for the spin-allowed ²B_{1g} → ²A_{1g} transition. This transition was characteristic of square planar geometry around the copper metal center. The observed magnetic moment values ranged from 1.43 to 1.47 B.M, indicating one unpaired electron on the copper metal center [47].

3.6. Fluorescence spectra.

The fluorescence spectra of all the compounds were recorded at room temperature in DMSO (Figure 6). Ligand shows an emission band at 461 nm with an excitation wavelength of 280 nm. The metal complexes displayed transitions at 479 nm, 518 nm, 520 nm, and 488 nm for cobalt, nickel, copper, and zinc, respectively. For 1:2 metal complexes, transitions appeared at 512 nm, 511 nm, 512 nm, and 452 nm for cobalt, nickel, copper, and zinc, respectively. All the metal complexes (1:1 and 1:2) showed enhanced fluorescence compared to the ligand.

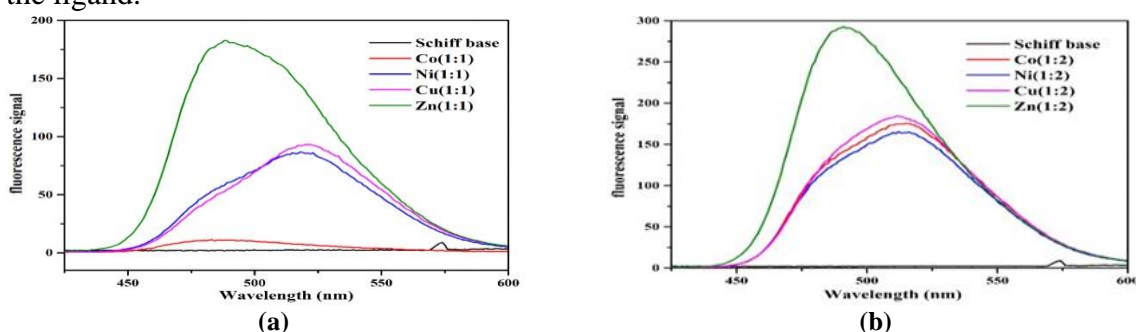


Figure 6. Fluorescence spectra of the ligand and its 1:1 (6a) and 1:2 (6b) metal complexes.

The increased emission indicates the complexation of the ligand with the metal ions and, hence, the fluorescence [48].

3.7. Thermal analysis.

The thermal analysis of 1:1 metal complexes was checked in the range of 40-1000°C with a heating rate of 10°C/min. On decomposition, the percentage mass loss, temperature range, decomposition moiety, and residue left were calculated and given in Table 5. After decomposition, the products are the respective metal oxides.

Table 5. The thermal decomposition step results in mass loss and residue left of the metal complexes.

Complexes	Temperature (°C)	Mass loss (%)		Decomposed moiety	Residue
		Calcd	Found		
Co(1:1)	70-120	10.24	11.02	3H ₂ O	CoO
	180-515	46.29	45.44	Organic moiety	
	550-750	32.47	31.50	Pyrazole moiety	
Ni(1:1)	70-195	10.24	10.81	3H ₂ O	NiO
	200-535	46.29	46.12	Organic moiety	
	545-765	32.47	31.89	Pyrazole moiety	
Cu(1:1)	65-120	3.63	4.61	H ₂ O	CuO
	140-515	49.22	48.24	Organic moiety	
	560-760	34.53	33.97	Pyrazole moiety	
Zn(1:1)	70-180	10.11	10.75	3H ₂ O	ZnO
	195-495	45.73	44.67	Organic moiety	
	540-765	32.08	30.99	Pyrazole moiety	

The thermal decomposition of Co(1:1) takes place in three steps. In the first step, three coordinated water molecules decompose in the temperature range of 70-120°C, with a percentage mass loss of 11.02% (calcd 10.24%). The second step involves the dissociation of the organic part, with a mass loss of 45.44% (calcd 46.29%) in the temperature range of 180-515°C. In the last step, the dissociation of the pyrazole moiety takes place with a mass loss of 31.50 % (calcd 32.47 %) in the temperature range 550-750°C. The residue left is CoO.

The thermal degradation of Ni(1:1) takes place in three major steps. In the initial step, the decomposition of three coordinated H₂O molecules occurs in the temperature range of 70-195°C, with a percentage mass loss of 10.81% (calculated 10.24%). The second step involves the dissociation of the organic moiety, with a mass loss of 46.12 % (calcd 46.29 %) in the temperature range of 200-535°C. In the last step, the dissociation of the pyrazole moiety occurs with a mass loss of 31.89 % (calcd 32.47 %) in the temperature range of 545-765°C. The residue left is NiO.

The thermal decomposition of Cu(1:1) takes place in three steps. In the first step, the decomposition of one coordinated water molecule occurs in the temperature range of 65-120 °C, with a percentage mass loss of 4.61% (calcd 3.63%). The second step involves the dissociation of the organic part with a mass loss of 48.24 % (calcd 49.22 %) in the temperature range of 140-515°C. In the last step, the dissociation of the pyrazole moiety occurs with a mass loss of 33.97 % (calcd 34.53 %) in the temperature range 550-760°C. The residue left is CuO.

The thermal degradation of Zn(1:1) takes place in three major steps. In the initial step, three coordinated H₂O molecules decompose in the temperature range of 70-180°C, with a percentage mass loss of 10.75% (calculated 10.11%). The second step involves the dissociation of the organic moiety, with a mass loss of 45.73 % (calcd 44.67 %) in the temperature range of 195-495°C. In the last step, the dissociation of the pyrazole moiety occurs

with a mass loss of 30.99 % (calcd 32.08 %) in the temperature range 540-765°C. The residue left is ZnO.

3.8. ESR Spectra.

The X-band ESR spectra of copper complexes give an idea about the no. of unpaired electrons and their geometry, as shown in the figure below. For the Cu(1:1) complex, the calculated g values follow the trend g_{\parallel} (2.217) > g_{\perp} (2.055) > g_e (2.0023). These values indicate that $2B_{1g}$ is the ground state, with the unpaired electron in an orbital, and that the copper metal ions are square planar [49]. There is significant copper-copper interaction, which was ensured by G values calculated by the equation:

$$G = \frac{(g_{\parallel} - 2.0023)}{(g_{\perp} - 2.0023)}$$

Covalent bonding in Cu(II)-ligand bond is considered on account of $g_{\parallel} < 2.3$. Molecular orbital coefficients α^2 (in-plane σ bonding), γ^2 (out-of-plane π -bonding), and β^2 (in-plane π -bonding) parameters were calculated with the help of ESR parameters. The detected α^2 value (0.316 for 1:1 and 0.4027 for 1:2) points toward the presence of appreciable covalency in the σ bond. β^2 (0.249 and 0.301) values show an interaction in the in-plane π -bonding, and γ^2 (0.254 for 1:1 and 0.267 for 1:2) values show an interaction in the out-of-plane π -bonding [50]. Parallel and perpendicular components of the orbital reduction factor follow the order $K_{\parallel} < K_{\perp}$ for the present Cu(1:1) complex, describing the higher contribution of in-plane π -bonding than out-of-plane.

π -bonding in metal-ligand bond and vice-versa in Cu(1:2). In Cu(1:2), the perceived g values are g_{\parallel} (2.210) > g_{\perp} (2.061) > g_e (2.0023), which suggests a square planar geometry of the complex and is consistent with a $2B_{1g}$ ground state with an unpaired electron in a n orbital. The G-value (3.53) is < 4, showing considerable exchange coupling in copper complexes (Figure 7).

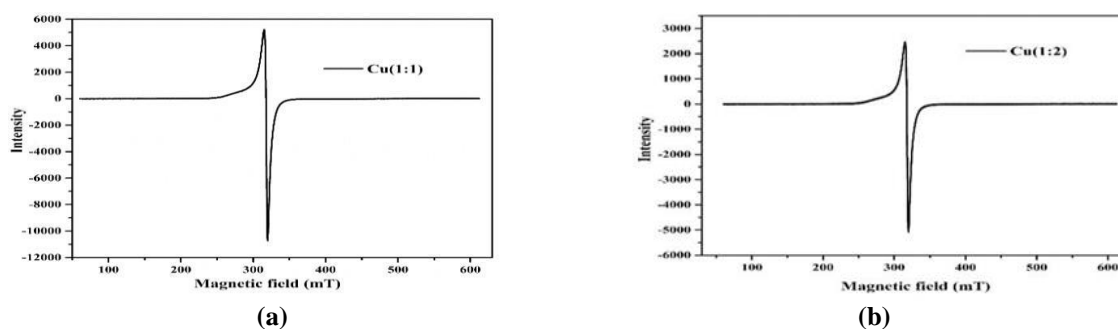


Figure 7. ESR spectra of the Cu(1:1) (a) and Cu(1:2) complexes (b).

3.8. Electrochemistry.

Cyclic voltammetry was performed on both copper complexes in DMSO to examine their electrochemical behavior, using a Pt electrode and potassium chloride as the supporting electrolyte at a scan rate of 0.1 Vs⁻¹ at room temperature (Figure 8). This behavior was compared with that of Schiff base and other metal complexes. Zinc complexes were excluded from this study due to their stable oxidation state (Zn²⁺, 3d¹⁰), which makes the zinc metal center inactive to redox behavior. Cyclic voltammograms of copper complexes in the potential range -1.0 to 1.5 V show a well-defined redox process in Cu(1:1) corresponding to Cu⁺²/Cu⁺¹

couple at $E_{pc} = -0.162$ V and corresponding anodic peak at $E_{pa} = 0.026$ V for Cu^{+1}/Cu^{+2} . For Cu(1:2), an anodic peak at $E_{pa} = 0.268$ V and an associated cathodic peak at $E_{pc} = 0.276$ V were observed. The ΔE_p values of 0.188 V and 0.008 V, respectively, for the 1:1 and 1:2 copper complexes indicated reversible behavior. Ratios of anodic peak currents to cathodic peak currents [$I_a/I_c = 0.81$ and 0.76 for Cu(1:1) and Cu(1:2), respectively] are near one, which corresponds to a electron process [51].

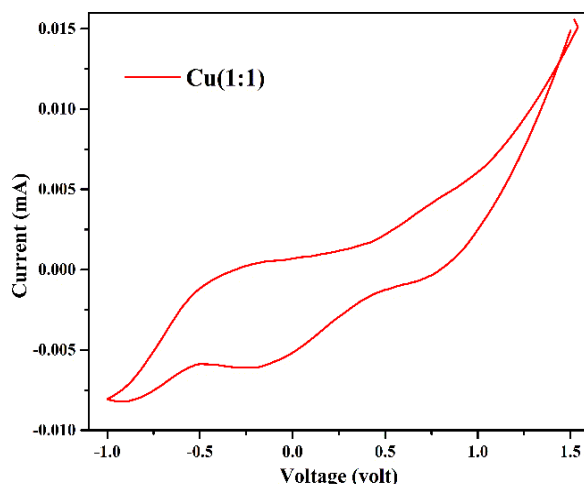


Figure 8. Cyclic voltammogram of the Cu(1:1) complex.

3.9. Biological activity.

All the compounds were tested for biological activity against several bacterial and fungal strains in DMSO. This may be due to Overtone's concept or Tweedy's chelation theory. Although all the complexes showed higher activity than the ligand, the zinc complexes exhibited the highest activity, with inhibition zones in the region 22-28 mm (Table 6 and Figure 9). The Ni(1:2) complex showed good activity against all bacteria except *C. perfringens*, with inhibition zones ranging from 21 to 22 mm. The Cu(1:2) metal complex displayed high activity against *S. aureus*, *C. perfringens*, and *P. aeruginosa*, with inhibition zone values of 20, 21, and 21 mm, respectively. Co(1:2) complex showed good activity against *S. aureus* (21 mm), *L. monocytogenes* (21 mm), *E. coli* (21 mm), and *P. aeruginosa* (20 mm). The results showed that the metal complexes exhibit enhanced biological activity compared to the parent ligand. The MIC values lie in the range 25-3.12 $\mu\text{g/mL}$ (Table 7 and Figure 10). Mycelial inhibition growth values range from 50.53% to 94.34%. The zinc metal complexes displayed high antifungal activity, with mycelial growth inhibition values ranging from 90.20 to 94.34 %.

Table 6. Inhibition zones of the compounds (mm).

Compound	<i>S. aureus</i>	<i>C. perfringens</i>	<i>L. monocytogenes</i>	<i>E. coli</i>	<i>P. aeruginosa</i>
Schiff base	15	17	14	14	15
Co(1:1)	19	18	21	19	17
Co(1:2)	21	18	21	21	20
Ni(1:1)	19	18	19	20	19
Ni(1:2)	22	18	21	22	21
Cu(1:1)	17	19	19	18	17
Cu(1:2)	20	21	18	19	21
Zn(1:1)	24	23	22	25	25
Zn(1:2)	28	25	24	25	27
Amikacin	30	21	25	22	23

The Cu(1:2) also showed good antifungal activity against all the fungi (88.08-90.00 %). Co(1:1) showed potent activity against *A. niger* and Co(1:2) against all fungi (Table 8 and Figure 11). Other metal complexes also showed good antifungal activity, with inhibition values higher than those of the ligand.

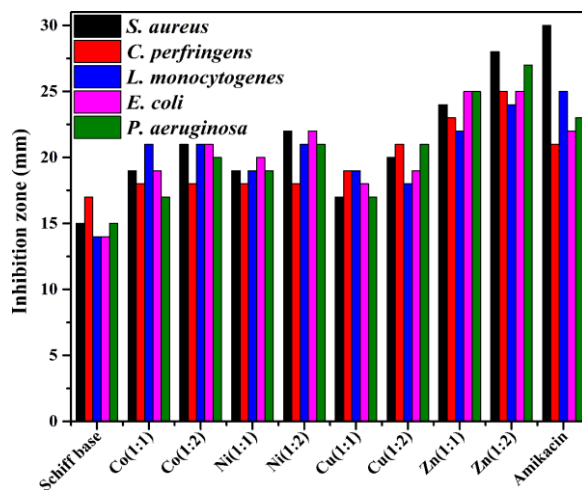


Figure 9. Inhibition zone of the compounds.

Table 7. MIC values of the ligand and its metal complexes ($\mu\text{g/mL}$).

Compound	<i>S. aureus</i>	<i>C. perfringens</i>	<i>L. monocytogenes</i>	<i>E. coli</i>	<i>P. aeruginosa</i>
Schiff base	25	12.5	25	25	25
Co(1:1)	12.5	12.5	6.25	12.5	12.5
Co(1:2)	6.25	12.5	6.25	6.25	12.5
Ni(1:1)	12.5	12.5	12.5	12.5	12.5
Ni(1:2)	6.25	12.5	6.25	6.25	6.25
Cu(1:1)	12.5	12.5	12.5	12.5	12.5
Cu(1:2)	12.5	6.25	12.5	12.5	6.25
Zn(1:1)	6.25	6.25	6.25	6.25	6.25
Zn(1:2)	3.12	6.25	6.25	6.25	3.12
Amikacin	3.12	6.25	6.25	6.25	6.25

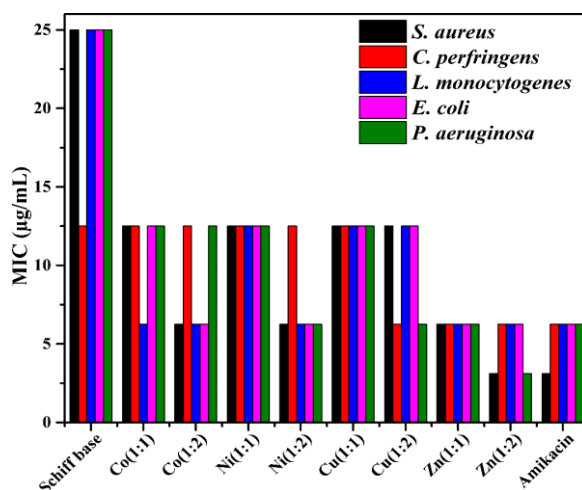


Figure 10. MIC values of the compounds.

Table 8. Mycelial growth inhibition values of the compounds (%).

Compound	<i>A. fumigatus</i>	<i>A. niger</i>	<i>C. albicans</i>
Schiff base	50.53	52.21	50.82
Co(1:1)	84.91	87.45	82.78
Co(1:2)	87.8	87.98	86.89
Ni(1:1)	76.32	81.86	79.32
Ni(1:2)	81.67	82.14	84.93
Cu(1:1)	86.99	87.75	87.7

Compound	<i>A. fumigatus</i>	<i>A. niger</i>	<i>C. albicans</i>
Cu(1:2)	90	88.88	88.08
Zn(1:1)	91.11	90.2	90.9
Zn(1:2)	92.84	93.61	94.34
Streptomycin	85.57	86.18	87.71

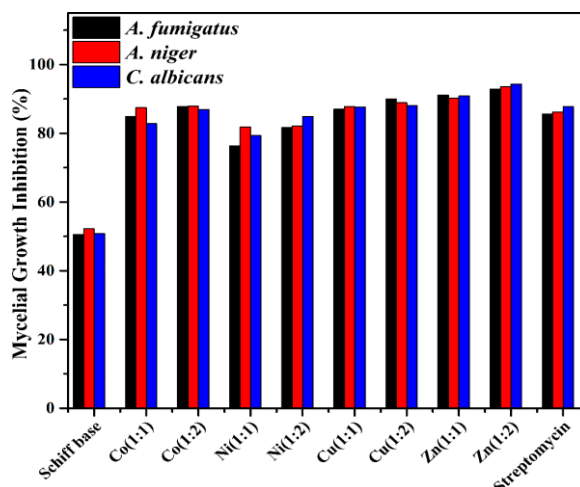


Figure 11. Mycelial growth inhibitions of the compounds.

4. Conclusions

In conclusion, a novel bioactive Schiff base (HL) has been synthesized by refluxing 5-amino-3-methyl-1-phenylpyrazole with 5-bromosalicylaldehyde. This Schiff base was characterized by ¹H-NMR and IR spectra. Its metal complexes with Co⁺², Ni⁺², Cu⁺², and Zn⁺² have also been synthesized. The characterization of the metal complexes was performed using various physicochemical techniques, including ¹H-NMR, UV-visible, IR, electronic spectra, electron spin resonance, cyclic voltammetry, and thermogravimetric analysis. The mode of coordination of ligands with the metal ions was explained with the help of IR spectroscopy. Schiff base binds to the metal ions in a bidentate fashion, i.e., the oxygen (O) of the hydroxy group and the nitrogen (N) of the imine moiety. The fluorescence spectra of all the synthesized compounds have been recorded, and the data indicate that the metal complexes exhibit an enhanced fluorescence signal compared to the ligand. The presence of coordinated water within or outside the coordination sphere was confirmed by thermogravimetric analysis. The geometries suggested for the cobalt, nickel, and zinc metal complexes are octahedral, and for the copper complexes are square planar. All the compounds were assessed in the biological assay, and the results revealed that the metal complexes exhibited better biological activity than the ligand.

Author Contributions

Conceptualization, P.D., K.S.; methodology, K.S.; software, P.D.; validation, P.D., K.S.; formal analysis, P.D.; investigation, P.D.; resources, P.D.; data curation, P.D.; writing—original draft preparation, P.D.; writing—review and editing, K.S., P.D.; visualization, P.D.; supervision, K.S.; project administration, P.D.; funding acquisition, P.D. All authors have read and agreed to the published version of the manuscript.

Institutional Review Board Statement

Not applicable.

Informed Consent Statement

Not applicable.

Data Availability Statement

Data supporting the findings of this study are available upon reasonable request from the corresponding author.

Funding

We give special thanks to the Department of Chemistry, Kurukshetra University, Kurukshetra, India, for providing research facilities, and to CSIR, New Delhi, India, for financial support in the form of a Junior Research Fellowship (JRF).

Acknowledgments

We give special thanks to the Department of Chemistry, Kurukshetra University, Kurukshetra,

Conflicts of Interest

The authors declare no conflict of interest.

References

1. Foster, T.J. Plasmid-determined resistance to antimicrobial drugs and toxic metal ions in bacteria. *Microbiol. Rev.* **1983**, *47*, 361–409, <http://doi.org/10.1128/mmbr.47.3.361-409.1983>.
2. Normark, B.H.; Normark, S. Evolution and spread of antibiotic resistance. *J. Intern. Med.* **2002**, *252*, 91–106, <https://doi.org/10.1046/j.1365-2796.2002.01026.x>.
3. Čulić, O.; Eraković, V.; Parnham, M.J. Anti-inflammatory effects of macrolide antibiotics. *Eur. J. Pharmacol.* **2001**, *429*, 209–229, [https://doi.org/10.1016/S0014-2999\(01\)01321-8](https://doi.org/10.1016/S0014-2999(01)01321-8).
4. Cook, J.; Baverstock, T.C.; McAndrew, M.B.L.; Stansfeld, P.J.; Roper, D.I.; Crow, A. Insights into bacterial cell division from a structure of EnvC bound to the FtsX periplasmic domain. *Proc. Natl. Acad. Sci. U.S.A.* **2020**, *117*, 28355–28365, <https://doi.org/10.1073/pnas.2017134117>.
5. Fu, Y.; Li, J.; Cai, W.; Huang, Y.; Liu, X.; Ma, Z.; Tang, Z.; Bian, X.; Zheng, J.; Jiang, J.; Li, C. The emerging tumor microbe microenvironment: From delineation to multidisciplinary approach-based interventions. *Acta Pharm. Sin. B* **2024**, *14*, 1560–1591, <https://doi.org/10.1016/j.apsb.2023.11.018>.
6. Uddin, M.N.; Ahmed, S.S.; Alam, S.M.R. REVIEW: Biomedical applications of Schiff base metal complexes. *J. Coord. Chem.* **2020**, *73*, 3109–3149, <https://doi.org/10.1080/00958972.2020.1854745>.
7. Abdel-Rahman, L.H.; Adam, M.S.S.; Al-Zaqri, N.; Shehata, M.R.; El-Sayed Ahmed, H.; Mohamed, S.K. Synthesis, characterization, biological and docking studies of ZrO(II), VO(II) and Zn(II) complexes of a halogenated tetra-dentate Schiff base. *Arab. J. Chem.* **2022**, *15*, 103737, <https://doi.org/10.1016/j.arabjc.2022.103737>.
8. Sumrra, S.H.; Habiba, U.; Zafar, W.; Imran, M.; Chohan, Z.H. A review on the efficacy and medicinal applications of metal-based triazole derivatives. *J. Coord. Chem.* **2020**, *73*, 2838–2877, <https://doi.org/10.1080/00958972.2020.1839751>.
9. Krishna, G.A.; Dhanya, T.M.; Shanty, A.A.; Raghu, K.G.; Mohanan, P.V. Transition metal complexes of imidazole derived Schiff bases: Antioxidant/anti-inflammatory/antimicrobial/enzyme inhibition and cytotoxicity properties. *J. Mol. Struct.* **2023**, *1274*, 134384, <https://doi.org/10.1016/j.molstruc.2022.134384>.
10. Keter, F.K.; Darkwa, J. Perspective: the potential of pyrazole-based compounds in medicine. *BioMetals* **2012**, *25*, 9–21, <https://doi.org/10.1007/s10534-011-9496-4>.
11. Keri, R.S.; Chand, K.; Ramakrishnappa, T.; Nagaraja, B.M. Recent Progress on Pyrazole Scaffold-Based Antimycobacterial Agents. *Arch. Pharm.* **2015**, *348*, 299–314, <https://doi.org/10.1002/ardp.201400452>.
12. Ribeiro, N.; Roy, S.; Butenko, N.; Cavaco, I.; Pinheiro, T.; Alho, I.; Marques, F.; Avecilla, F.; Costa Pessoa,

- J.; Correia, I. New Cu(II) complexes with pyrazolyl derived Schiff base ligands: Synthesis and biological evaluation. *J. Inorg. Biochem.* **2017**, *174*, 63–75, <https://doi.org/10.1016/j.jinorgbio.2017.05.011>.
13. Chalkha, M.; Moussaoui, A.E.; Hadda, T.B.; Berredjem, M.; Bouzina, A.; Almalki, F.A.; Saghrouchni, H.; Bakhouch, M.; Saadi, M.; Ammari, L.E.; Abdellatif, M.H.; Yazidi, M.E. Crystallographic study, biological evaluation and DFT/POM/Docking analyses of pyrazole linked amide conjugates: Identification of antimicrobial and antitumor pharmacophore sites. *J. Mol. Struct.* **2022**, *1252*, 131818, <https://doi.org/10.1016/j.molstruc.2021.131818>.
 14. Tigreros, A.; Portilla, J. Recent progress in chemosensors based on pyrazole derivatives. *RSC Adv.* **2020**, *10*, 19693–19712, <https://doi.org/10.1039/d0ra02394a>.
 15. Al Zoubi, W.; Al-Hamdani, A.A.S.; Ahmed, S.D.; Ko, Y.G. Synthesis, characterization, and biological activity of Schiff bases metal complexes. *J. Phys. Org. Chem.* **2018**, *31*, e3752, <https://doi.org/10.1002/poc.3752>.
 16. Gupta, V.; Kant, V. A Review on Biological Activity of Imidazole and Thiazole Moieties and Their Derivatives. *Sci. Int.* **2013**, *1*, 253–260, <https://doi.org/10.17311/sciintl.2013.253.260>.
 17. Tariq, S.; Wani, S.; Rasool, W.; Shafi, K.; Bhat, M.A.; Prabhakar, A.; Shalla, A.H.; Rather, M.A. A comprehensive review of the antibacterial, antifungal and antiviral potential of essential oils and their chemical constituents against drug-resistant microbial pathogens. *Microb. Pathog.* **2019**, *134*, 103580, <https://doi.org/10.1016/j.micpath.2019.103580>.
 18. Zarenezhad, E.; Farjam, M.; Iraj, A. Synthesis and biological activity of pyrimidines-containing hybrids: Focusing on pharmacological application. *J. Mol. Struct.* **2021**, *1230*, 129833, <https://doi.org/10.1016/j.molstruc.2020.129833>.
 19. Shakir, M.; Hanif, S.; Sherwani, M.A.; Mohammad, O.; Al-Resayes, S.I. Pharmacologically significant complexes of Mn(II), Co(II), Ni(II), Cu(II) and Zn(II) of novel Schiff base ligand, (E)-N-(furan-2-yl methylene) quinolin-8-amine: Synthesis, spectral, XRD, SEM, antimicrobial, antioxidant and *in vitro* cytotoxic studies. *J. Mol. Struct.* **2015**, *1092*, 143–159, <https://doi.org/10.1016/j.molstruc.2015.03.012>.
 20. Ashraf, T.; Ali, B.; Qayyum, H.; Haroone, M.S.; Shabbir, G. Pharmacological aspects of schiff base metal complexes: A critical review. *Inorg. Chem. Commun.* **2023**, *150*, 110449, <https://doi.org/10.1016/j.inoche.2023.110449>.
 21. He, Y.; Wang, Z.; Wang, H.; Wang, Z.; Zeng, G.; Xu, P.; Huang, D.; Chen, M.; Song, B.; Qin, H.; Zhao, Y. Metal-organic framework-derived nanomaterials in environment related fields: Fundamentals, properties and applications. *Coord. Chem. Rev.* **2021**, *429*, 213618, <https://doi.org/10.1016/j.ccr.2020.213618>.
 22. Sağlam, S.; Türk, F.N.; Arslanoğlu, H. Use and applications of metal-organic frameworks (MOF) in dye adsorption: Review. *J. Environ. Chem. Eng.* **2023**, *11*, 110568, <https://doi.org/10.1016/j.jece.2023.110568>.
 23. Dilshad, K.A.J.; Rabinal, M.K. Review on Molecularly Controlled Design of Electrodes for Metal–Air Batteries: Fundamental Concepts and Future Directions. *Energy Fuels* **2023**, *37*, 5689–5711, <https://doi.org/10.1021/acs.energyfuels.2c04147>.
 24. Low, M.L.; Paulus, G.; Dorlet, P.; Guillot, R.; Rosli, R.; Delsuc, N.; Crouse, K.A.; Polcar, C. Synthesis, characterization and biological activity of Cu(II), Zn(II) and Re(I) complexes derived from S-benzylthiocarbamate and 3-acetylcoumarin. *BioMetals* **2015**, *28*, 553–566, <https://doi.org/10.1007/s10534-015-9831-2>.
 25. Ghorai, P.; Saha, R.; Bhuiya, S.; Das, S.; Brandão, P.; Ghosh, D.; Bhaumik, T.; Bandyopadhyay, P.; Chattopadhyay, D.; Saha, A. Syntheses of Zn(II) and Cu(II) Schiff base complexes using N,O donor Schiff base ligand: Crystal structure, DNA binding, DNA cleavage, docking and DFT study. *Polyhedron* **2018**, *141*, 153–163, <https://doi.org/10.1016/j.poly.2017.11.041>.
 26. Kargar, H.; Fallah-Mehrjardi, M.; Behjatmanesh-Ardakani, R.; Munawar, K.S.; Ashfaq, M.; Tahir, M.N. Synthesis, spectral characterization, SC-XRD, HSA, DFT and catalytic activity of a dioxidomolybdenum complex with aminosalicyl-hydrazone Schiff base ligand: An experimental and theoretical approach. *Polyhedron* **2021**, *208*, 115428, <https://doi.org/10.1016/j.poly.2021.115428>.
 27. Kargar, H.; Ardakani, A.A.; Tahir, M.N.; Ashfaq, M.; Munawar, K.S. Synthesis, spectral characterization, crystal structure and antibacterial activity of nickel(II), copper(II) and zinc(II) complexes containing ONNO donor Schiff base ligands. *J. Mol. Struct.* **2021**, *1233*, 130112, <https://doi.org/10.1016/j.molstruc.2021.130112>.
 28. Deswal, Y.; Asija, S.; Tufail, A.; Dubey, A.; Deswal, L.; Kumar, N.; Kirar, J.S.; Gupta, N.M.; Barwa, P. Metal Complexes of 1,2,4-Triazole Based Ligand: Synthesis, Structural Elucidation, DFT Calculations, Alpha-Amylase and Alpha-Glucosidase Inhibitory Activity Along with Molecular Docking Studies. *J.*

- Inorg. Organomet. Polym. Mater.* **2024**, *34*, 144–160, <https://doi.org/10.1007/s10904-023-02808-4>.
29. Agarwal, P.; Asija, S.; Deswal, Y.; Kumar, N. Recent advancements in the anticancer potentials of first row transition metal complexes. *J. Indian Chem. Soc.* **2022**, *99*, 100556, <https://doi.org/10.1016/j.jics.2022.100556>.
 30. Deswal, Y.; Asija, S.; Dubey, A.; Deswal, L.; Kumar, D.; Kumar Jindal, D.; Devi, J. Cobalt(II), nickel(II), copper(II) and zinc(II) complexes of thiadiazole based Schiff base ligands: Synthesis, structural characterization, DFT, anti-diabetic and molecular docking studies. *J. Mol. Struct.* **2022**, *1253*, 132266, <https://doi.org/10.1016/j.molstruc.2021.132266>.
 31. Deswal, Y.; Asija, S.; Kumar, D.; Jindal, D.K.; Chandan, G.; Panwar, V.; Saroya, S.; Kumar, N. Transition metal complexes of triazole-based bioactive ligands: synthesis, spectral characterization, antimicrobial, anticancer and molecular docking studies. *Res. Chem. Intermed.* **2022**, *28*, 703–729, <https://doi.org/10.1007/s11164-021-04621-5>.
 32. Deswal, Y.; Asija, S.; Tufail, A.; Dubey, A.; Deswal, L.; Kumar, N.; Saroya, S.; Kirar, J.S.; Gupta, N.M. Instigating the in vitro anti-diabetic activity of new tridentate Schiff base ligand appended M(II) complexes: From synthesis, structural characterization, quantum computational calculations to molecular docking, and molecular dynamics simulation studies. *Appl. Organomet. Chem.* **2023**, *37*, e7050, <https://doi.org/10.1002/aoc.7050>.
 33. Abdel-Rahman, L.H.; Al-Farhan, B.S.; Al Zamil, N.O.; Noamaan, M.A.; El-Sayed Ahmed, H.; Adam, M.S.S. Synthesis, spectral characterization, DFT calculations, pharmacological studies, CT-DNA binding and molecular docking of potential N, O-multidentate chelating ligand and its VO(II), Zn(II) and ZrO(II) chelates. *Bioorg. Chem.* **2021**, *114*, 105106, <https://doi.org/10.1016/j.bioorg.2021.105106>.
 34. Ossai, V.; Obiefuna, A.P.; Laraps, B.C.; Okenyeka, O.U.; Ezeorah, J.C.; Dege, N.; Ibezim, A.; Lutter, M.; Jurkschat, K.; Obasi, N.L. Crystal structural and *in silico* studies of Schiff bases derived from 4-aminoantipyrine. *Solid State Sci.* **2020**, *106*, 106293, <https://doi.org/10.1016/j.solidstatesciences.2020.106293>.
 35. Saritha, T.J.; Metilda, P. Synthesis, spectroscopic characterization and biological applications of some novel Schiff base transition metal (II) complexes derived from curcumin moiety. *J. Saudi Chem. Soc.* **2021**, *25*, 101245, <https://doi.org/10.1016/j.jscs.2021.101245>.
 36. Makode, J.T.; Yaul, A.R.; Bhadange, S.G.; Aswar, A.S. Physicochemical characterization, thermal, and electrical conductivity studies of some transition metal complexes of bis-chelating Schiff base. *Russ. J. Inorg. Chem.* **2009**, *54*, 1372–1377, <https://doi.org/10.1134/S003602360909006X>.
 37. Bolos, C.A.; Nikolov, G.S.; Ekateriniadou, L.; Kortsaris, A.; Kyriakidis, D.A. Structure-Activity Relationships for Some Diamine, Triamine and Schiff Base Derivatives and Their Copper(II) Complexes. *Met. Based. Drugs* **1998**, *5*, 323–332, <https://doi.org/10.1155/MBD.1998.323>.
 38. Asadi, M.; Khah, M.S. Some new unsymmetrical diimino tetradentate schiff base derived from 3,4-Diaminobenzophenone: Synthesis, characterization and the formation constant of Ni(II) and Cu(II) complexes. *J. Iran. Chem. Soc.* **2010**, *7*, 875–882, <https://doi.org/10.1007/BF03246082>.
 39. Devi, P.; Singh, K.; Makawana, D. Novel Pyrazole-Based Transition Metal Complexes: Spectral, Photophysical, Thermal and Biological Studies. *Chem. Biodivers.* **2023**, *20*, e202300072, <https://doi.org/10.1002/cbdv.202300072>.
 40. Sujamol, M.S.; Athira, C.J.; Sindhu, Y.; Mohanan, K. Synthesis, spectroscopic characterization, dyeing performance and corrosion inhibition study of transition metal complexes of a novel azo derivative formed from 2-aminothiophene. *Chem. Data Collect.* **2021**, *31*, 100634, <https://doi.org/10.1016/j.cdc.2020.100634>.
 41. Azam, M.; Mohammad Wabaidur, S.; Alam, M.; Trzesowska-Kruszynska, A.; Kruszynski, R.; Al-Resayes, S.I.; Fahhad Alqahtani, F.; Rizwan Khan, M.; Rajendra. Design, structural investigations and antimicrobial activity of pyrazole nucleating copper and zinc complexes. *Polyhedron.* **2021**, *195*, 114991, <https://doi.org/10.1016/j.poly.2020.114991>.
 42. Singh, K.; Turk, P.; Dhanda, A. Synthesis, spectral characterization, and antimicrobial evaluation of new imine derived from 3-methylthiophene-2-carboxaldehyde and its Co(II), Ni(II), Cu(II), and Zn(II) metal complexes. *Appl. Organomet. Chem.* **2021**, *35*, e6088, <https://doi.org/10.1002/aoc.6088>.
 43. Gavisiddegowda, P.; Rajashekhar, D.N.; Kollur, S.P.; Doddarevanna, R.H. Biological Potency of New Benzimidazole Derived Imine Based Ligand and its Co (III), Ni (II), Cu (II) and Pt (II) Complexes: Synthesis, Structure, Antimicrobial, Antioxidant and BSA Interaction Studies. *Biointerface Res. Appl. Chem.* **2021**, *11*, 11856-11890, <https://doi.org/10.33263/BRIAC114.1185611890>.
 44. Alhakimi, A.N.; Shakhdofo, M.M.E.; Saeed, S.; Shakhdofo, A.M.E.; Al-Fakeh, M.S.; Abdu, A.M.; Alhagri, I.A. Transition Metal Complexes Derived from 2-hydroxy-4-(p-tolyldiazenyl) benzylidene)-2-(p-

- tolylamino) acetohydrazide Synthesis, Structural Characterization, and Biological Activities. *J. Korean Chem. Soc.* **2021**, *65*, 93–105, <https://doi.org/10.5012/jkcs.2021.65.2.93>.
45. Singh, K.; Kumari, B.; Sharma, A. Copper(II), nickel(II), zinc(II) and cadmium(II) complexes of 1,2,4-triazole based Schiff base ligand: synthesis, comparative spectroscopic, thermal, biological and molecular docking studies. *Spectrosc. Lett.* **2021**, *54*, 742–762, <https://doi.org/10.1080/00387010.2021.1996395>.
 46. Fouad, R.; Shaaban, I.A.; Aliba, T.E.; Assiri, M.A.; Shenouda, S.S. Co(II), Ni(II), Cu(II) and Cd(II)-thiocarbonohydrazone complexes: spectroscopic, DFT, thermal, and electrical conductivity studies. *RSC Adv.* **2021**, *11*, 37726–37743, <http://doi.org/10.1039/D1RA06902K>.
 47. Hashem, H.E.; Mohamed, E.A.; Farag, A.A.; Negm, N.A.; Azmy, E.A.M. New heterocyclic Schiff base-metal complex: Synthesis, characterization, density functional theory study, and antimicrobial evaluation. *Appl. Organomet. Chem.* **2021**, *35*, e6322, <https://doi.org/10.1002/aoc.6322>.
 48. Song, H.; Liu, G.; Fan, C.; Pu, S. A novel fluorescent sensor for Al³⁺ and Zn²⁺ based on a new europium complex with a 1,10-phenanthroline ligand. *J. Rare Earths.* **2021**, *39*, 460–468, <https://doi.org/10.1016/j.jre.2020.02.020>.
 49. Kavitha, N.; Lakshmi, P. V. A.; Synthesis, characterization and thermogravimetric analysis of Co(II), Ni(II), Cu(II) and Zn(II) complexes supported by ONNO tetradentate Schiff base ligand derived from hydrazino benzoxazine. *J. Saudi Chem. Soc.* **2017**, *21*, S457–S466, <https://doi.org/10.1016/j.jscs.2015.01.003>.
 50. Devi, P.; Singh, K.; Kubavat, B. Synthesis, spectroscopic, quantum, thermal and kinetics, antibacterial and antifungal studies: Novel Schiff base 5-methyl-3-((5-bromosalicylidene) amino)- pyrazole and its transition metal complexes. *Res. Chem.* **2023**, *5*, 100813, <https://doi.org/10.1016/j.rechem.2023.100813>.
 51. Devi, P.; Singh, K.; Dabas, P. Synthesis of Co⁺², Ni⁺², Cu⁺², and Zn⁺² complexes of Schiff base 5-methyl-3-((3,5-dichlorosalicylidene) amino)-pyrazole, spectral, and biological studies. *J. Coord. Chem.* **2022**, *75*, 162–177, <https://doi.org/10.1080/00958972.2022.2035726>.

Publisher's Note & Disclaimer

The statements, opinions, and data presented in this publication are solely those of the individual author(s) and contributor(s) and do not necessarily reflect the views of the publisher and/or the editor(s). The publisher and/or the editor(s) disclaim any responsibility for the accuracy, completeness, or reliability of the content. Neither the publisher nor the editor(s) assume any legal liability for any errors, omissions, or consequences arising from the use of the information presented in this publication. Furthermore, the publisher and/or the editor(s) disclaim any liability for any injury, damage, or loss to persons or property that may result from the use of any ideas, methods, instructions, or products mentioned in the content. Readers are encouraged to independently verify any information before relying on it, and the publisher assumes no responsibility for any consequences arising from the use of materials contained in this publication.